

Slip flow and wall depletion layer of microfibrillated cellulose suspensions in a pipe flow

Antti Koponen¹, Sanna Haavisto², Juha Salmela², and Markku Kataja³

¹VTT Technical Research Centre of Finland Ltd, P.O. Box 1603, 40101 Jyväskylä, Finland
²Spinnova Ltd, Finland

³University of Jyväskylä, P.O. Box 35, FI-40014 Jyväskylä, Finland

ABSTRACT

Rheological properties and boundary layer flow behaviour of Micro Fibrillated Cellulose (MFC) suspended in water was studied using Ultrasound Velocity Profiling (UVP) and Optical Coherence Tomography (OCT). The high-resolution OCT provided velocity profiles near the transparent tube wall, while UVP yielded corresponding information in the interior parts of the flow. The results from interior part of the flow showed typical power law shear thinning behaviour of MFC suspension. Close to the wall the suspension was found to have strong (apparent) slip flow associated with depletion of MFC particles from the wall. In this thin depletion layer the consistency and the viscosity of the suspension decrease rapidly with decreasing distance from the wall. In the immediate vicinity of the wall the viscosity of the suspension was found to be close to that of pure water.

INTRODUCTION

As potential ingredients for novel bio-based materials and high-end products, Microfibrillated Cellulose (MFC) materials are subject of active research and of commercial interest within forest industry. Often, production and processing of MFC involves the fibrous MFC material suspended in a carrier fluid, typically water. Similar to many other natural and synthetic fiber suspensions, the rheological and flow properties of aqueous MFC suspensions are

diverse, and depend strongly on the fiber properties and fiber mass concentration.

Conventional experimental techniques for measuring rheological properties of fluids are typically based on simple and well-defined flow geometries where the flow condition is assumed known. Such presumptions are, however, questionable in the case of complex heterogeneous fluids and the obtained parameters may lack generality^{1 2 3}.

The crux of velocity profiling rheometry is to combine conventional rheological techniques and simultaneous measurement of flow velocity profile⁴. The data analysis can then be based on a measured instead of assumed velocity profile. Velocity profiling techniques applicable for turbid fluids are e.g. Magnetic Resonance Imaging (MRI), Ultrasound Velocity profiling⁵ (UVP) and Optical Coherence Tomography⁶ (OCT). Due to their lower spatial resolution, MRI and UVP can be used in the inner parts of the flowing geometry whereas OCT can be used to measure the flow in the vicinity of the walls of the flowing geometry.

In this work we report results on rheological and boundary layer flow properties of a MFC suspension utilizing velocity profiling. The velocity profile is measured by combining data from simultaneous measurements by OCT and UVP. The combination of data from these instruments provides a comprehensive velocity profile including both the boundary layer and the inner regions of the tube.

MATERIALS AND METHODS

Materials

The microfibrillated cellulose used in this work was obtained from Daicel Chemical Industries, Japan. The product type was Celish KY-100G, which is manufactured mechanically from purified wood pulp. The average length and diameter of the fibers are 8 μm and 60 nm, respectively⁷. The final MFC suspensions used in the flow experiments were obtained by diluting the original MFC by deionized water to mass consistencies of 0.4%, 1.0% and 1.6%.

Experimental setup

The measurement unit consisted of a 2.5 m long optical grade glass tube with an inner radius of $R = 9.5$ mm. The flow in the tube was driven by a low-pulsation progressive cavity pump. The fluid temperature in the loop was set to 21°C with a digital temperature control unit. The volumetric flow rate in the loop was measured using a magnetic flow rate sensor. The measurements were carried out at stationary flow conditions in the flow rate range of 8 – 160 ml/s. The wall shear stress at each flow rate was obtained with two pressure difference sensors with a separation of 1.0 m. The measurement setup has been explained in more detail in Kataja et al.⁸ and Haavisto et al.⁹.

Ultrasound velocity profiling

Ultrasound Velocity Profiling (UVP) is a well-established experimental technique in applications of fluid dynamics and engineering involving flow measurements⁵. It is based on using an emitter-receiver probe to send a series of short ultrasound bursts into the flow, and detecting the echoes issuing from target particles moving along with the flow. In this work UVP was used in

measuring the flow velocity profile in the main part of the pipe diameter. However, the results obtained near the wall were rejected due to uncertainties caused by wall interference typical to UVP method¹⁰.

Optical coherence tomography

Optical Coherence Tomography (OCT) is a light-based imaging method, which enables measurement of flow fields in scattering opaque materials with micron-scale spatial resolution⁶. OCT uses interference of a low coherence light to record depth-dependent reflectivity and velocity profiles. In this work OCT was used for measuring the velocity profile near the tube wall where UVP is not applicable.

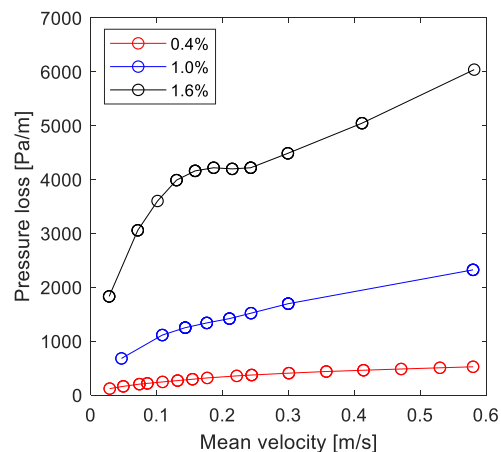


Figure 1. Measured pressure loss vs. flow rate for MFC suspension at various consistencies.

RESULTS

Pressure loss and velocity profiles

Fig. 1 shows the measured pressure loss as a function of mean velocity for all three consistencies studied. The pressure drop curves resemble typical behaviour of shear thinning fluids. For 1.6% MFC, pressure loss temporarily levels in a narrow mean velocity range around 0.2 m/s. This phenomenon, typical to drag reduction, is caused by the

(apparent) wall slip; similar behaviour is also observed with other fiber suspensions ¹¹.

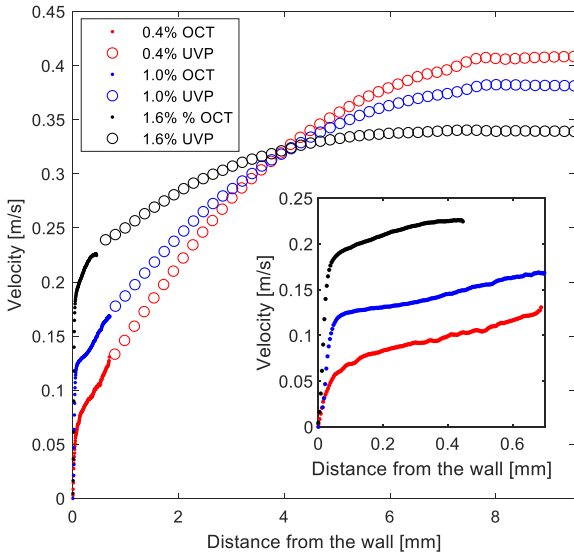


Figure 2. The velocity profiles of MFC suspensions between tube wall and centre line as measured by UVP and OCT at mean flow velocity of 0.3 m/s. The inset shows the OCT velocity profiles in more detail.

Fig. 2 shows examples of measured stationary UVP and OCT velocity profiles. In most cases studied in this work, the velocity profiles measured by OCT in the near wall region and by UVP in the interior parts of the tube showed overlapping region of mutually consistent results. Notice that a normalization procedure, based on independently measured flow rate, was used to avoid inaccuracies due to uncertainty of the used values of UVP and OCT Doppler angles ⁸.

In Fig. 2, the overall velocity profile appears to include two dynamically different parts. In the interior part of the tube, at the distance range of $200 \mu\text{m} \lesssim y \leq R$, the profile is relatively shallow and qualitatively resembles that of a shear thinning fluid with wall slip. The high-resolution OCT data shown in more detail in the inset of Fig. 2 reveals, however, that in a thin near-wall region, the velocity profile is very steep and approaches rapidly zero towards the wall. No actual wall slip is thus observed.

Rheological properties of MFC suspension

The measured UVP velocity profiles $u(y)$ were used to calculate the viscosity of the MFC suspension in the interior parts of the tube, where consistency of the suspension is constant with a value close to its mean value. The local value of viscosity is given by

$$\mu(y) = \frac{\tau(y)}{\dot{\gamma}(y)}, \quad (1)$$

where, $\dot{\gamma} = du(y)/dy$ and $\tau(y) = \tau_w(1 - y/R)$ are the local shear rate and shear stress at distance y from the wall, respectively. Moreover, $\tau_w = R\nabla p/2$ is the wall shear stress obtained from the measured pressure gradient ∇p .

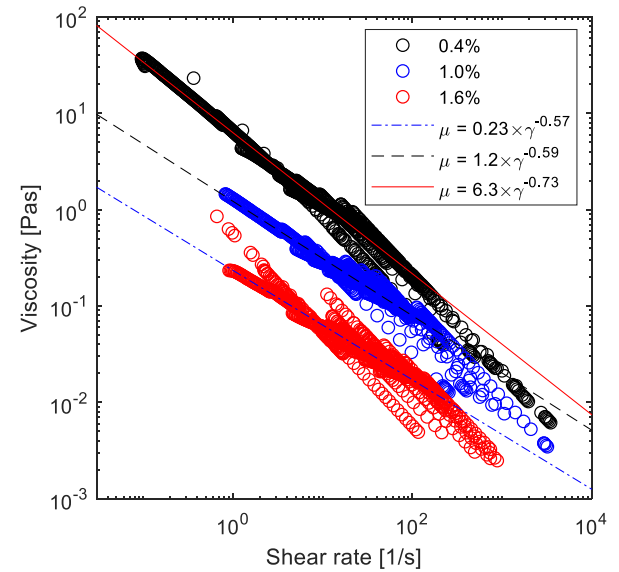


Figure 3. Viscosity of MFC suspension at various consistencies as a function of shear rate, calculated locally from the measured UVP velocity profiles. Straight lines show fits of power law Eq. (2) to the data.

Fig. 3 shows the values of viscosity vs. shear rate, obtained from Eq. (1), for all values of flow rate measured and for the three values of consistency. MFC suspensions are

generally considered as power-law fluids¹²
¹³. The straight lines shown in Fig. 3 are fits of the formula

$$\mu = K\dot{\gamma}^{n-1}, \quad (2)$$

to the measured data. In Eq. (2) parameter K is the *consistency index* and parameter n is the *flow index*. Table 1 collects the fitted values of these parameters at various consistencies. Notice that magnetic resonance imaging (data not shown) gave almost identical values for these parameters.

Table 1. Consistency index K , flow index n and critical drag reduction shear stress τ_{DR} at various MFC consistencies c . The value of τ_{DR} for 0.4% MFC is the wall shear stress at which the wall viscosity saturates.

According to

c [%]	K	n	τ_{DR} [Pa]
0.4	0.23	0.43	(1)
1	1.2	0.41	7
1.6	6.3	0.27	20

The dependence of consistency index K and flow index n on the MFC consistency c can also be fitted by a power law with a reasonable degree of correlation. The results are

$$K = 1.7 \times c^{2.3} \quad (3)$$

and

$$n = 0.35 \times c^{-0.31} \quad (4)$$

with the coefficient of determination $R^2 = 0.97$ and $R^2 = 0.69$ for the consistency index and the flow index, respectively. The values of the exponents in Eqs. (3) and (4) are in accordance with earlier studies^{13 14 15 16}. By combining Eqs. (2), (3) and (4) we get

$$\mu(c, \dot{\gamma}) = 1.7c^{2.3}\dot{\gamma}^{0.35c^{-0.31}-1}. \quad (5)$$

In Eq. (5) the dependence of the MFC viscosity on consistency and shear rate is expressed in a single formula. It is used below to calculate consistency profiles of MFC close to the pipe wall from the OCT data.

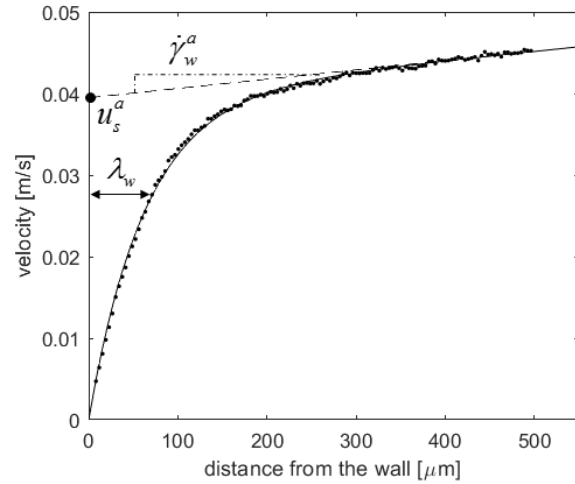


Figure 4. Example of a fitted velocity profile Eq. (6) to a measured OCT velocity profile. Also shown is the graphical interpretation of the three free fitting parameters.

Notice that in addition to experimental uncertainties, Eq. (5) has some limitations. Firstly, the definite upper limit for shear rate is obtained when viscosity in Eq. (5) is that of water, $\mu \sim 1$ mPas, i.e. when $\dot{\gamma}_{max} = 93900 \times c^{1.67}$. The theoretical maximum shear rate is thus very high, and the viscosity of the MFC suspension saturates with shear rate values clearly below $\dot{\gamma}_{max}$. Kumar et al.¹⁷ studied MFC viscosity in a 1 mm slit flow with shear rates of 100 - 100000 1/s. According to their results viscosity seemed to saturate at shear rates 15000 1/s and 20000 1/s for consistencies 1.0% and 2.0%, respectively. In the current work the highest shear rate values were measured for 1.6% MFC suspension. Shear rate values in excess of 10000 1/s were obtained, however, only at distances smaller than 10 μ m from the wall. Another limitation of Eq. (5) is that below the gel point, which for this MFC is ca. 0.2%⁷, the suspension is nearly Newtonian

and the consistency dependence of viscosity is weaker. According to Geng et al.¹⁸ viscosity is proportional to $c^{0.4}$ in the consistency range 0.01 - 0.2% and to $c^{2.3}$ at higher values of consistency. These results are in qualitative agreement with the present results.

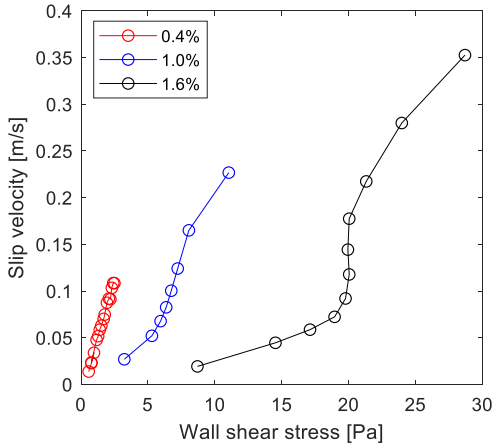


Figure 5. Apparent slip velocity as a function of wall shear stress.

Parametrization of velocity profiles

Fig. 4 shows an example of a measured OCT velocity profile together with a fit of the functional form

$$u(y) = \dot{\gamma}_w^a y + u_s^a (1 - e^{-y/\lambda_w}) \quad (6)$$

to the measured data. Here, the parameter λ_w characterizes the thickness of the wall boundary layer underlying the apparent wall slip. The parameters u_s^a and $\dot{\gamma}_w^a$ can be interpreted as the apparent slip velocity and the apparent wall shear rate, respectively. As obvious from these definitions the term 'apparent' is used here to refer to wall quantities observable in the macroscopic scales and related to the velocity profile shape well outside the boundary layer, the very existence of which may be difficult to observe without a specific technique such as OCT. Using these parameters, we can calculate the local viscosity of the suspension from

$$\mu(y) = \frac{\tau(y)}{\dot{\gamma}_w^a + u_s^a e^{-y/\lambda_w} / \lambda_w} \quad (7)$$

The measured OCT velocity profiles could be quite well approximated by Eq. (6) with all the flow rates and consistencies used. (The same functional form has been used successfully also for a clearly finer MFC grade¹⁹.) To improve accuracy, the analysis below is based on values of fitting parameters obtained by averaging over up to four independent OCT measurements.

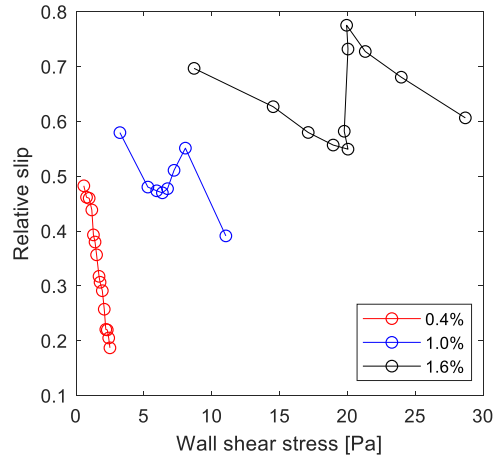


Figure 6. Relative slip as a function of wall shear stress.

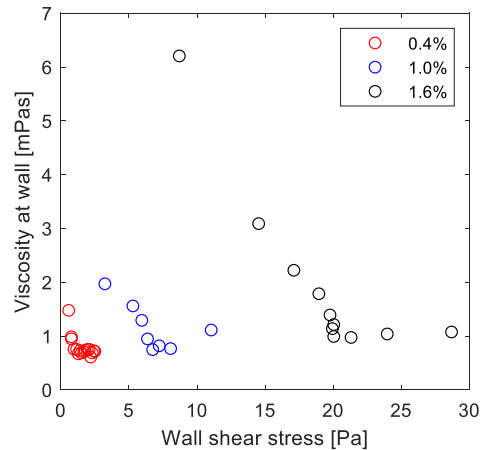


Figure 7. The measured values of viscosity at tube wall $y = 0$ as a function of wall shear stress.

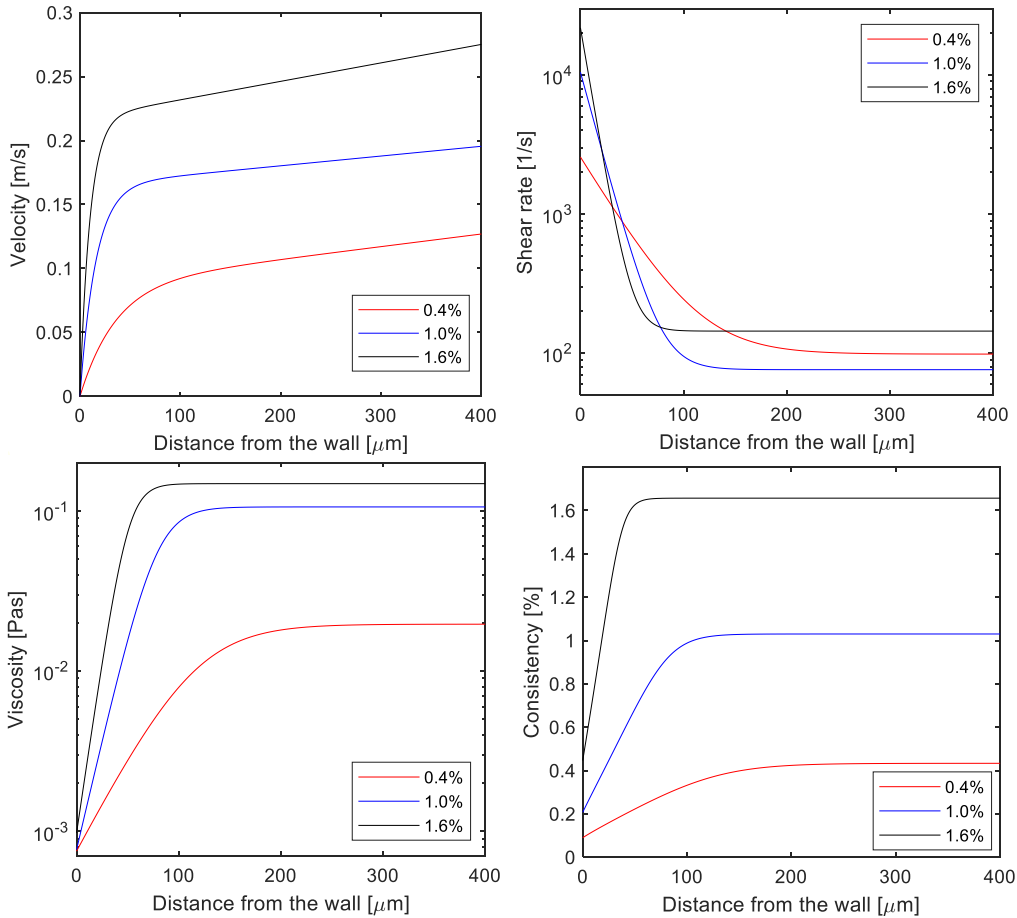


Figure 8. a) Velocity, b) shear rate, c) viscosity, and d) consistency profiles near the tube wall for MFC suspensions at mean flow velocity 0.3 m/s and at various mean consistencies. The results are calculated using the parametrized velocity profiles and viscosity correlations based on measured OCT velocity profiles and pressure loss data.

Fig. 5 shows the apparent slip velocity as a function of wall shear stress. Slip is seen to increase monotonously with increasing shear stress. For 1.6% MFC there is a narrow shear stress region where the slip-shear stress curve becomes almost vertical.

Fig. 6 shows the *relative slip*, *i.e.* the contribution of slip to the total flow rate, as a function of wall shear stress. We see that relative slip first decreases with increasing shear stress. Then, at a *critical drag reduction shear stresses*, τ_{DR} , of 7 Pa and 20 Pa, relative slip increases rapidly for consistencies of 1.0% and 1.6%, respectively. Interestingly, the viscosity at the wall becomes constant at τ_{DR} being

approximately that of water, *i.e.* $\mu_w \sim 1$ mPas (see Fig. 7). This happens also for 0.4% MFC suspension at $\tau_w \sim 1$ Pa. The observed strong slip flow (see Fig. 6) and the low value of viscosity at the wall (Fig. 7) are most likely related to existence of a consistency gradient near the wall. The well-known explanation for such phenomenon is given by the combined effect of steric hindrance and repulsive hydrodynamic interaction between the tube wall and suspended particles^{20 21 22}. Notice that for the given MFC τ_{DR} has been found to be approximately two times the yield stress²³.

Analysis of velocity profiles

Figs. 8a and 8b show the parametrized velocity profiles and shear rate profiles for the measured OCT profiles shown in Fig. 2. The viscosity profiles shown in Fig. 8c and the consistency profiles shown in Fig. 8d were calculated from Eq. (7) and Eq. (5), respectively. Near the wall, the consistency increases almost linearly with distance from the wall, but levels off to the average consistency of the suspension outside of the wall depletion layer. On the other hand, at the wall $\mu_w \sim 1$ mPas (see Fig. 7), and $\mu_w \rightarrow \mu_c$ far away from the wall. This viscosity value, valid in the central parts of the tube, can be roughly estimated using the correlations discussed above. This leads to

$$\mu_c = K(\tau_w/K)^{1-1/n}, \quad (8)$$

where the values of coefficients K and n are obtained from Eqs. (3) and (4), respectively, using the mean value of consistency. Notice however that the calculated value of consistency at the wall remains well above zero for all three values of mean consistency. This apparent discrepancy is likely to be due to experimental inaccuracies and the limitations of Eq. (5) as discussed above. Subject to experimental uncertainties, the consistency profiles of 0.4% MFC were rather similar with all flow rates. With higher consistencies the thickness of the consistency profiles varied with flow rate (see below). In the literature, the wall depletion layer of MFC suspension is often envisaged simply as a layer of pure water with thickness

$$\delta_w = \frac{v_s \mu_0}{\tau_w}, \quad (9)$$

where μ_0 is the viscosity of water and v_s is the slip velocity¹⁷. However, as we see in Fig. 8d, MFC consistency increases gradually in the wall depletion layer. According to the present result, the wall layer thickness is characterized by parameter λ_w

introduced in Eq. (6). Using Eq. (7) and the result that $\mu = \mu_w$ at $y = 0$, and $\mu \approx \mu_c$ when $y \gg \lambda_w$, we obtain

$$\lambda_w = \frac{v_s \mu_w}{\tau_w (1 - \mu_w / \mu_c)}. \quad (10)$$

Notice that when shear stress exceeds τ_{DR} , we have $\mu_w \sim 1$ mPas, and λ_w can be calculated from Eq. (10) provided that the slip velocity and the viscosity parameters K and n are known.

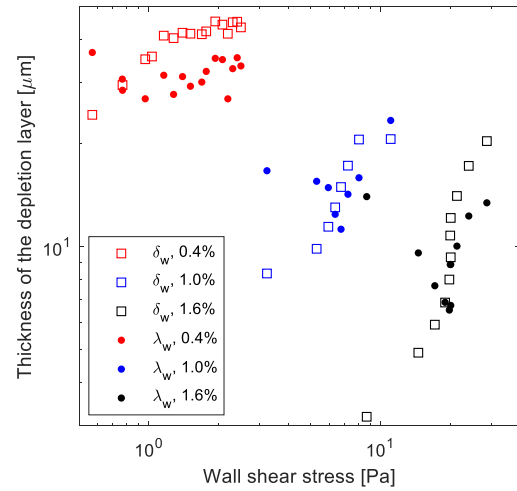


Figure 9. Values of the thickness of the wall depletion layer δ_w , given by Eq. (9), and the parameter λ_w , given by Eq. (10).

Fig. 9 shows the thickness of the wall depletion layer δ_w given by Eq. (9) and λ_w given by Eq. (10) as a function of wall shear stress. We see that the magnitude of δ_w and λ_w is similar in each case, their qualitative dependence on wall shear stress, and thus on *e.g.* flow rate, is quite different. While δ_w increases monotonously with increasing shear stress, parameter λ_w varies showing minimum at the critical drag reduction shear stress τ_{DR} .

We finally notice that Eqs. (8) and (10) also yield slip velocity as

$$v_s = \frac{\lambda_w \tau_w (1 - \mu_w / K (\tau_w / K)^{1-1/n})}{\mu_w}. \quad (12)$$

While v_s depends linearly on λ_w , the dependence on μ_w and τ_w is highly nonlinear. Equation (12) is useful e.g. in estimating the effect of various flow parameters on the magnitude of slip flow.

CONCLUSIONS

Optical Coherence Tomography (OCT) and Ultrasound Velocity Profiling (UVP) were used to study the rheological properties and boundary layer behavior of MFC suspension flow in a straight tube at consistencies 0.4%, 1.0%, and 1.6%. The two velocity profiling methods are complementary - OCT technique is capable of high-resolution measurement of the boundary layer flow very close to the tube wall while the UVP method is useful in measuring the velocity profile in the interior parts of the tube with lower spatial resolution.

In the interior parts of the tube where the MFC consistency is constant, in average, the results show typical shear thinning behavior. The near wall behavior shows existence of a boundary layer where the mean concentration decreases towards the wall. Such a concentration gradient leads to apparent wall slip at the wall. The thickness of the boundary layer decreases with MFC concentration. With increasing flow rate (wall shear stress), the fluid next to the tube wall may become nearly Newtonian with viscosity close to that of water.

ACKNOWLEDGMENTS

The authors highly appreciate collaboration with UC Davis, in particular with professors Michael J. McCarthy and Robert L. Powell. This project has received funding from the EU's Horizon 2020 programme under grant agreement No 713475. This work is a part of the Academy of Finland's Flagship Programme under Project No. 318891.

OPEN DATA: 10.5281/zenodo.3338084

REFERENCES

1. Nechyporchuk, O. et al. *Carbohydr. Polym.* 112, 432–439 (2014).
2. Saarinen, T. et al. *Cellulose* 21, 1261–1275 (2014).
3. Naderi, A. & Lindström, T. *Cellulose* 31, 3507–3514 (2016).
4. Powell, R. *Phys. Fluids* 20, 040605–22 (2008).
5. *Ultrasonic Doppler velocity profiler for fluid flow.* (Springer Japan, 2012).
6. *Optical coherence tomography, technology and applications.* (Springer, 2008).
7. Varanasi, S., He, R. & Batchelor, W. *Cellulose* 20, 1885–1896 (2013).
8. Kataja, M. et al. *Nord. Pulp Pap. Res. J.* 32, 473–482 (2017).
9. Haavisto, S. et al. *Exp. Fluids* 58, (2017).
10. Kotzé et al., *Ultrasonics* 53, 459–469 (2013).
11. Lee, P. & Duffy, G. *Appita* 30, 219–226 (1976).
12. Honorato, C. et al. *J. Mater. Sci.* 50, 7343–7352 (2015).
13. Schenker, et al. *Cellulose* 25, 961–976 (2018).
14. Lasseguette, E., Roux, D. & Nishiyama, Y. *Cellulose* 15, 425–433 (2008).
15. Mohtaschemi, M. et al. *Cellulose* 21, 3913–3925 (2014).
16. Nazari, et al. *J. Rheol.* 60, 1151 (2016).
17. Kumar et al. *Applied Rheology* 26, 1–11 (2016).
18. Geng, L. et al. in *Nanocelluloses: Their Preparation, Properties, and Applications* 113–132 (American chemical society, 2017).
19. Lauri, J. et al. *Cellulose* 24, 4715–4728 (2017).
20. Barnes, H. *Journal of Non-Newtonian Fluid Mechanics* 56, 221–251 (1995).
21. Medhi, et al. *Int. J. Multiph. Flow* 37, 609–619 (2011).
22. Jäsberg et al. *Comput. Phys. Commun.* 129, 196–206 (2000).
23. Haavisto et al., *TAPPI Journal* 14 (5), 291–302 (2015).